Motion Compensation Strategies in Tomography

Bernadette N. Hahn

Abstract Imaging modalities have been developed and established as important and powerful tools to recover characteristics of the interior structure of a studied specimen from induced measurements. The reconstruction process constitutes a well-known application of the theory of inverse problems and is well understood if the investigated object is stationary.

However, in many medical and industrial applications, the studied quantity shows a time-dependency, for instance due to patient or organ motion. Most imaging modalities record the data sequentially, i.e. temporal changes of the object during the measuring process lead to inconsistent data sets. Therefore, standard reconstruction techniques which solve the underlying inverse problem in the static case lead to motion artefacts in the computed image and hence to a degraded image quality.

Consequently, suitable models and algorithms with a specific treatment of the dynamics have to be developed in order to solve such time-dependent imaging problems. This article provides a respective theoretical framework as well as numerical results from different imaging applications, including a study of 3D cone-beam CT.

1 Motivation and State-of-the-Art

Over the past decades, tomographic techniques have been developed and established as powerful and important tools for non-invasive imaging with various applications from clinical diagnosis to non-destructive testing. Exploiting the properties of an imaging agent, e.g. propagation of electromagnetic waves, the induced response from a studied medium is measured. The reconstruction of the searched-for function, characteristic of the medium, from the collected data thus matches with solving an associated inverse problem. If the object under investigation is stationary

B. N. Hahn (✉)
Department of Mathematics, University of Stuttgart, Stuttgart, Germany
e-mail: bernadette.hahn@imng.uni-stuttgart.de
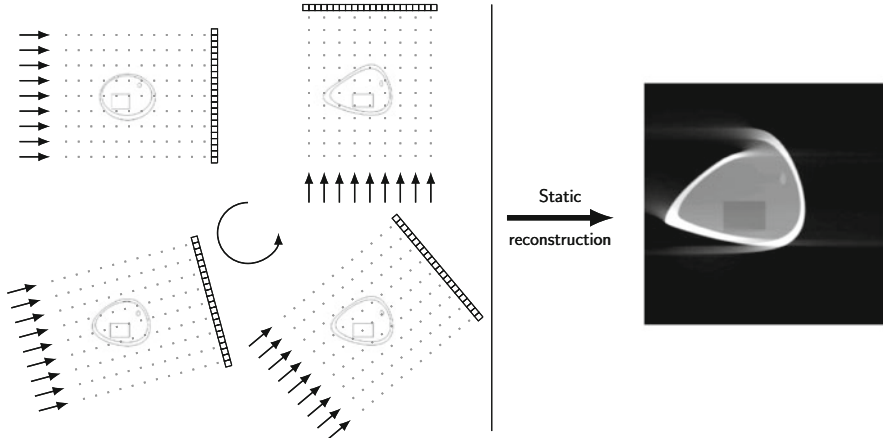
Fig. 1 Temporal changes of a specimen during the data acquisition in computerized tomography (left) and standard reconstruction applied to dynamic data (right)

during the time-dependent scanning, the reconstruction process is well known for most of the imaging systems, see [37].

However, the stationary-assumption is often not satisfied. Prominent examples arise in medical imaging due to respiratory and cardiac motion, gastrointestinal motility, blood flow or body movement of Parkinson patients or infants. Besides clinical applications, investigating dynamic objects arouses the interest in non-destructive testing such as imaging driven liquid fronts for oil recovery studies [2], performing elasticity experiments during the scan to determine material parameters [22], or imaging objects in working stage, e.g. aircraft engines [5].

The dynamic behaviour of the investigated object during the data collection leads to an inconsistent data set. Therefore, standard reconstruction techniques which solve the underlying inverse problem in the static case lead to motion artefacts in the computed image (e.g. blurring, ghosting, distortions) which can significantly degrade the image quality and hence misleads the diagnosis [12, 27, 47], see also Fig. 1. For hybrid imaging methods, these artefacts lead to spatial misalignments of the reconstructions which significantly reduce the diagnostic accuracy and hence affect the success of the treatment [36].

Dynamic Inverse Problems
Following [44], we refer to an inverse problem, where the investigated object is allowed to change during the measuring process, as *dynamic inverse problem*.

1.1 Hardware-Based Artefact Reduction Strategies

In medical imaging, the periodic nature of physiologic motion can be exploited to reduce motion artefacts by hardware-based gating methods. External devices, e.g. electrocardiographs and thoracic belts, detect respiratory expansion and/or cardiovascular motion, and are then used to collect and assort the measured data to specific phases in the motion cycle [9, 13]. A main drawback of the described artefact reduction procedures is their restriction to periodic (patient) motion and hence, it cannot be extended e.g. to applications in non-destructive testing.

Another, intuitive approach is to reduce the required data acquisition time for individual imaging modalities by faster scanners or reduced sampling in data space. In [42], and recently in [38], a multi-source computerized tomography set-up is proposed to avoid the time-consuming rotation of a single radiation source. However, this decreases the signal-to-noise-ratio and hence the quality of the reconstructed image.

1.2 Reconstruction Techniques for Motion Compensation

A more general approach is provided by *motion compensation* methods, where the dynamical information is incorporated in the reconstruction step.

For individual imaging modalities like CT, MRI or PET, several methods of this type have been proposed in the literature, see below for an overview.

Gating methods in general neglect the strong temporal correlation between the single phases. By taking temporal redundancies into account, the reconstruction step can be formulated as a variational problem [10, 39]. If explicit deformation models are incorporated, e.g. in terms of an optimal flow constraint or shape information, this approach leads to non-convex optimization problems [3–5, 28, 29].

For special deformations which preserve the underlying data acquisition geometry, exact analytic reconstruction methods have been derived, especially in computerized tomography, where this type of motion includes affine deformations, [7, 8, 14, 43]. In this case, techniques for rebinning the measured data to make them feasible for standard reconstruction methods are proposed as well, [5, 34]. Besides iterative methods, e.g. [1, 21], approximate inversion formulas have been derived in computerized tomography to compensate for general, non-affine deformations [23, 24].

So far, only a few regularization techniques have been developed in the general context of dynamic linear inverse problems [25, 44, 45], which have been applied in computerized and impedance tomography, respectively. The more recent article [6] proposes a computational method in a Bayesian framework along with an approach to quantify uncertainties of the obtained solution. However, especially the method in [44, 45], suffers from high computational costs and the motion artefacts are not entirely eliminated.

1.3   Outline of the Article

This article is devoted to the study of regularization methods for dynamic inverse problems, summarizing the theoretical framework provided in [14–16] and presenting novel numerical results from various imaging applications. More precisely, we study the application of our theory in the context of photoacoustic tomography and 3D cone-beam CT, whereas the mentioned previous articles evaluated the respective theory at the example of 2D computerized tomography with parallel scanning geometry.

In Sect. 2, we incorporate the time-dependency of the investigated object in the inverse problem associated to the static case by means of diffeomorphic motion models. We then provide an overview of strategies to estimate the motion information from the measured data, which allows to assume the motion to be known prior to the actual reconstruction step.

The resulting mathematical model of dynamic inverse problems gives then rise to a classification scheme distinguishing two cases depending on the object's motion. Section 3 summarizes a general regularization theory for the first category of *moderate deformations*, a subclass of affine deformations, which was developed in detail in [16]. The theoretical results are evaluated at an example from photoacoustic tomography.

For the more general second category of *strong deformations*, a regularization strategy is developed in Sect. 4 by extending the *method of the approximate inverse* to the time-dependent setting as initially proposed in [15]. The design of efficient algorithms is discussed and evaluated at the example of 3D cone-beam computerized tomography.

2   The Mathematical Model of Dynamic Inverse Problems

This section is devoted to the derivation of suitable mathematical models for dynamic inverse problems with a specific treatment of the dynamics.

First, we derive a motion model based on the physical observation that the particles forming the material body change their position in space over time. An object which is changing in time is described by a sequence of functions $f_t : \mathbb{R}^n \to \mathbb{R}$, $t \in [0, T] \subset \mathbb{R}$, representing the different configurations over time. Thus, the motion can be described by a sequence of displacements which correlate the different states of the body to one reference configuration. In particular, this motion model corresponds to the *Lagrangian description* which gives the trajectory of each material particle starting from the initial position [48].

Finally, the model describing the dynamic inverse problem is obtained by combining the motion model with the forward operator from the underlying static scenario.
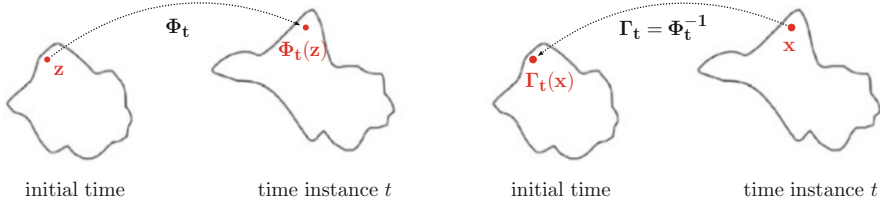
Fig. 2 Illustration of the motion model in terms of Φ_t (left) and Γ_t (right)

2.1 Diffeomorphic Motion Models

Throughout the article, let $[0, T] \subset \mathbb{R}$ denote an interval covering the time period required for the measurement process. Without loss of generality, we consider the initial state of the object, denoted by f_0, as the reference configuration represented in the cartesian coordinate system of $\mathbb{R}^n$. The motion of the particles can then be expressed by a sequence of mappings $\Phi_t : \mathbb{R}^n \to \mathbb{R}^n$, $t \in [0, T]$ with $\Phi_0(x) = x$. Considering the particle initially located at position $x \in \mathbb{R}^n$, the vector $\Phi_t(x)$ denotes its position at time t, see Fig. 2 (left).

Motivated by medical applications and elastic deformations in non-destructive testing, Φ_t is assumed to be a diffeomorphism for all $t \in [0, T]$ and we denote $\Gamma_t := \Phi_t^{-1}$. The descriptive interpretation of the mapping Γ_t is the following: The particle located at x at time t was at the initial time at position $\Gamma_t x$, see Fig. 2 (right).

Using the *motion functions* Γ_t, $t \in [0, T]$ and the initial state function f_0, we find the state of the object at time instance t to be

$$f(t, x) = f_0(\Gamma_t(x)). \tag{1}$$

To simplify the notation, we write $\Gamma_t x$ instead of $\Gamma_t(x)$.

Remark 1 This motion model is intensity preserving, i.e. each particle keeps its initial intensity over time. Analogously, a mass preserving model of type

$$f(t, x) = f_0(\Gamma_t x) \, | \det D\Gamma_t x|$$

could be considered. Please note that this simply results in different weights within the mathematical model of dynamic inverse problems. In particular, this does not alter the nature of our reconstruction algorithms, as explained in [18].

Support Condition

In applications, the studied specimen, more precisely f_0 and all its transformed versions f_t, $t \in [0, T]$ typically have compact support. In particular,

(continued)

we assume

$$\text{supp}(f_0(\Gamma_t \cdot)) \subset \Omega_X \quad \text{for all } t \in [0, T] \tag{2}$$

with a bounded subset $\Omega_X \subset \mathbb{R}^n$. Further, throughout the article, we make use of the continuous extension $f_0(x) := 0$ for $x \notin \Omega_X$.

We next address how such motion information can be extracted from measured data.

Extraction of Motion Information

In applications, the exact motion, i.e. the motion functions $\Gamma_t : \mathbb{R}^n \to \mathbb{R}^n$, $t \in [0, T]$ are in general unknown. If modelled by suitable basis functions b_k, e.g. B-splines [50] with coefficients $w_k(t) \in \mathbb{R}$,

$$\Gamma_t(x) = \sum_{k=1}^{N} w_k(t) b_k(t, x),$$

this requires to estimate the paramters $w_k(t)$ prior to or within the reconstruction step.

Recovering both the unknown parameters and the reference image of the object simultaneously leads to non-convex optimization problems of extremely large size, [3]. This complexity however can be reduced by decoupling the two tasks.

For instance, the calibration of the deformation parameters is proposed to be performed via additional measurements with external devices or via additional images, eventually obtained from another imaging modality [1, 7, 35, 40, 41]. In [34], linear scaling and translation parameters are estimated directly from dynamic, two-dimensional CT-data without any prior knowledge about the object or any additional measurement. This approach is extended in [17] to general parametrized deformation maps. The authors in [24] propose an iterative procedure: If edges look cluttered in an initial reconstruction, the reconstruction step is repeated with an updated motion model.

In the following, we want to focus on the aspect of motion compensation. Therefore, throughout the article, we assume the deformation maps Γ_t, $t \in [0, T]$, to be known.

2.2 Model Operators for Dynamic Linear Inverse Problems

We now turn to the derivation of forward operators modelling dynamic inverse problems. To this end, we combine our motion model with the mathematical model that characterizes the underlying static case.

Many imaging modalities can be modelled mathematically by a linear integral operator represented by a kernel $k : [0, T] \times \mathbb{R}^m \times \mathbb{R}^n \to \mathbb{R}$ (or $\mathbb{C}$) via

$$\mathcal{A} : L_2(\Omega_X) \longrightarrow L_2([0, T] \times \Omega_Y)$$

$$\mathcal{A}h(t, y) = \int_{\mathbb{R}^n} h(x) \, k(t, y, x) \, \mathrm{d}x, \tag{3}$$

where Ω_X and Ω_Y denote bounded subsets of $\mathbb{R}^n$ and $\mathbb{R}^m$, respectively. In this model, the codomain of $\mathcal{A}$ is already given in the time-resolved form (i.e. the time instance t arises explicitly as one of the data variables) accounting for a time-dependent data acquisition. However, the investigated object described by h is assumed to be static. Therefore, we refer to the problem

$$\text{`` Find } h \text{ from } \mathcal{A}h(t, y) = g(t, y), \quad t \in [0, T], y \in \Omega_Y\text{''} \tag{4}$$

as *static inverse problem*.

Example (Static CT)

The mathematical model for 2D computerized tomography (CT) is given by the 2D Radon transform

$$\mathcal{R} : L_2(V_1(0)) \longrightarrow L_2([0, 2\pi] \times \mathbb{R})$$

$$\mathcal{R}h(\varphi, s) = \int_{\mathbb{R}^2} h(x) \, \delta(s - x^T \theta(\varphi)) \, \mathrm{d}x$$

with $\theta(\varphi) = (\cos(\varphi), \sin(\varphi))^T$, the delta-distribution δ and the unit circle $V_1(0)$. This model corresponds to the integration of the searched-for static quantity h, which is compactly supported in $V_1(0)$, along the straight lines

$$L(\varphi, s) := \{x \in \mathbb{R}^2 \, : \, x^T \theta(\varphi) = s\}. \tag{5}$$

In modern CT scanners, all detector points record simultaneously. Thus, the time consuming step of the data acquisition protocol is the rotation of the radiation source around the specimen. Since the source position is

(continued)

characterized by the angle φ, this is the data variable that can be uniquely identified by a time instance t and vice versa. Thus, the mapping

$$\mathcal{R} : L_2(V_1(0)) \longrightarrow L_2([0, 2\pi] \times \mathbb{R})$$

$$\mathcal{R}h(t, s) = \int_{\mathbb{R}^2} h(x)\, \delta(s - x^T \theta(t))\, \mathrm{d}x$$

matches the time-resolved representation (3).

We now derive the mathematical model for the associated time-dependent inverse problem. Let the sequence of functions $(f_t)_{t \in [0,T]}$, $f_t : \mathbb{R}^n \to \mathbb{R}$, characterize the time-dependent object with compact support in $\Omega_X \subset \mathbb{R}^n$. Then, at time instance t, the measurement $g(t, \cdot)$ encodes the state f_t. Thus, the associated dynamic inverse problem is given by

$$\mathcal{A}^{dyn} f(t, y) = g(t, y) \tag{6}$$

with the dynamic operator

$$\mathcal{A}^{dyn} f(t, y) := \mathcal{A} f_t(t, y)$$

and $f \in L_2([0, T] \times \Omega_X)$, $f(t, x) := f_t(x)$. Thus, $\mathcal{A}^{dyn}$ can be considered as mapping from $L_2([0, T] \times \Omega_X)$ into $L_2([0, T] \times \Omega_Y)$. If the static operator $\mathcal{A}$ is of type (3), then

$$\mathcal{A}^{dyn} f(t, y) = \int_{\mathbb{R}^n} f(t, x)\, k(t, y, x)\, \mathrm{d}x.$$

From this representation, it becomes clear that additional information are required in order to extract the time-dependent quantity f from the dynamic data $g = \mathcal{A}^{dyn} f$.

Additional Information Required

The added time dimension regarding the searched-for quantity results in an incomplete data problem: In the static case, all measured data, i.e. $g(t, \cdot)\, \forall\, t \in [0, T]$, encode the information about one single object state. For instance in CT, this corresponds to recovering a function from all its line integrals. In contrast, in the dynamic scenario, only a very small portion of the data, namely $g(t, \cdot)$ for one single time instance t, encode each individual state. In

(continued)

CT, this corresponds to the task of recovering each state f_t from a subset of its line integrals (namely only from line integrals in direction $\theta(t)^\perp$).

Thus, solving dynamic inverse problems typically requires the incorporation of some additional information. Hence, we now incorporate temporal correlations of the individual object states in terms of a motion model as described in Sect. 2.1.

Incorporating correlation (1), i.e. $f(t, x) = f_0(\Gamma_t x)$, in the definition of the dynamic forward operator $\mathcal{A}^{dyn}$, we obtain the following operator $\mathcal{A}_\Gamma$ for the initial state function

$$\mathcal{A}_\Gamma f_0(t, y) := \int_{\mathbb{R}^n} f_0(\Gamma_t x)\, k(t, y, x)\, \mathrm{d}x,$$

which depends on the motion functions Γ_t, $t \in [0, T]$. In particular, the substitution $x \mapsto \Gamma_t x$ yields the equivalent representation

$$\mathcal{A}_\Gamma f_0(t, y) = \int_{\mathbb{R}^n} |\det D\Gamma_t^{-1}(x)|\, f_0(x)\, k(t, y, \Gamma_t^{-1}x)\, \mathrm{d}x. \tag{7}$$

The support condition (2) ensures that the range $R(\mathcal{A}_\Gamma)$ is a subset of $L_2([0, T] \times \Omega_Y)$. Thus, $\mathcal{A}_\Gamma$ can be considered as mapping from $L_2(\Omega_X) \to L_2([0, T] \times \Omega_Y)$.

If the deformation fields Γ_t are known, the dynamic inverse problem (6) reduces to determining f_0 from the equation

$$\mathcal{A}_\Gamma f_0 = g. \tag{8}$$

Example (Dynamic CT)
In dynamic 2D CT, the inverse problem

$$\mathcal{R}_\Gamma f_0 = g$$

has to be solved with the dynamic forward operator

$$\mathcal{R}_\Gamma f_0(t, s) = \int |\det D\Gamma_t^{-1}x|\, f_0(x)\, \delta(s - (\Gamma_t^{-1}x)^T \theta(t))\, \mathrm{d}x.$$

This operator integrates a weighted version of the reference state f_0 along the curved lines

<div align="right">(continued)</div>

Fig. 3 Integration curves in
the static case (left) and in
case of a non-affine
deformation (right)
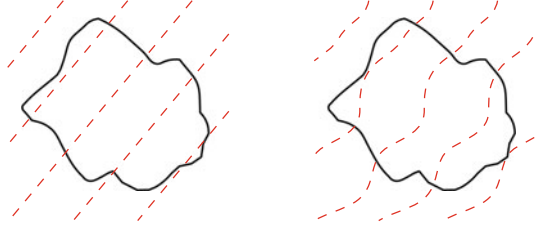
$$C_\Gamma(t, s) = \{x \in \mathbb{R}^2 \mid (\Gamma_t^{-1} x)^T \theta(t) = s\},$$

see also Fig. 3.

If the dynamic behaviour is described by affine deformations, i.e. $\Gamma_t x :=$ $A_t x + b_t$ with $A_t \in \mathbb{R}^{2\times 2}$ and $b_t \in \mathbb{R}^2$ for all $t \in [0, T]$, then the integration curves simplify to

$$C_{A_t, b_t}(t, s) = \{x \in \mathbb{R}^2 \mid x^T (A_t^T \theta(t)) = s + A_t^T b_t\}.$$

Thus, in this particular case, they correspond to shifted and rotated versions of the original straight lines $L(t, s)$ from the static case, see (5), and the dynamic operator $\mathcal{R}_\Gamma$ can be related to the underlying static operator $\mathcal{R}$ by a change of coordinates in data space. This means

$$\mathcal{R}_\Gamma = \mathcal{V} \mathcal{R}$$

with suitable transformation $\mathcal{V}$.

In general, however, it is not possible to express a curved line as rigid transformation of a straight line. In this case, the dynamic model $\mathcal{R}_\Gamma$ cannot be related to $\mathcal{R}$ by modifying the data acquisition scheme, so we can say *they differ strongly.*

This observation from dynamic CT motivates the following classification scheme for dynamic inverse problems.

Classification Scheme [16]

Let $\mathcal{A}$ be a static operator and let $(\Gamma_t)_{t \in [0,T]}$ be a motion model. If there exists a diffeomorphism $M : [0, T] \times \mathbb{R}^m \to [0, T] \times \mathbb{R}^m$ and a continuous function $\alpha : [0, T] \times \mathbb{R}^m \to [0, T] \times \mathbb{R}^m \setminus \{0\}$ such that

(continued)

$$\mathcal{A}_\Gamma = \mathcal{V}\mathcal{A}$$

with an operator

$$\mathcal{V}g(y) = \alpha(t, y)\, g(M(t, y)), \tag{9}$$

then the motion model $(\Gamma_t)_{t\in[0,T]}$ is called *moderate* with respect to $\mathcal{A}$. Otherwise, we speak of a *strong* motion model with respect to $\mathcal{A}$.

The operator $\mathcal{V}$ as in (9) is studied in more detail in Theorem 1.

Inverse problems, including (6) and (8), are in general ill-posed and thus, a regularization method is required to solve these problems. In the following sections, we address the derivation of suitable dynamic regularizations for both types of deformations.

We conclude this section by stating the representation of the adjoint operators $\mathcal{A}_\Gamma^*$ and $\mathcal{A}^{dyn*}$, since they play an important role throughout the article. For the time-resolved operator $\mathcal{A}^{dyn*}$, we calculate

$$\mathcal{A}^{dyn*}g(t, x) = \int_{\Omega_Y} \overline{k(t, y, x)}\, g(t, y)\, \mathrm{d}y.$$

A change of coordinates in the integral $\langle \mathcal{A}_\Gamma f, g\rangle_{L_2}$ leads to the representation

$$\mathcal{A}_\Gamma^* g(x) = \int_{[0,T]\times\Omega_Y} \overline{k(t, y, \Gamma_t^{-1}x)}\, g(t, y)\, \mathrm{d}t\, \mathrm{d}y. \tag{10}$$

If we denote

$$\mathcal{A}_t : L_2(\Omega_X) \longrightarrow L_2(\mathbb{R}^m)$$

$$f \mapsto \mathcal{A}_t f(y) := \mathcal{A}f(t, y)$$

for fixed $t \in [0, T]$, then, with

$$\mathcal{A}^* g(x) = \int_{[0,T]} \mathcal{A}_t^* g_t(x)\, \mathrm{d}t,$$

it holds

$$\mathcal{A}^{dyn*}g(x) = \mathcal{A}_t^* g_t(x), \tag{11}$$

and

$$\mathcal{A}_\Gamma^* g(x) = \int_{[0,T]} |\det D\Gamma_t^{-1} x|\, \mathcal{A}_t^* g_t(\Gamma_t^{-1} x)\, \mathrm{d}t \qquad (12)$$

for $g \in L_2([0, T] \times \mathbb{R}^m)$ with $g_t(y) := g(t, y)$.

With the mathematical model at hand, we now develop suitable regularization methods within the subsequent sections.

3   Compensating Moderate Deformations

In this section, we study regularization strategies for dynamic inverse problems with moderate motion. To this purpose, we consider the more general setting of $\mathcal{A}$ being a mapping into a weighted L_2-space, i.e.

$$\mathcal{A} : L_2(\Omega_X) \to L_2([0, T] \times \Omega_Y, w)$$

with a measurable weight w. Considering such weighted L_2-spaces has several advantages, for instance with respect to mapping properties or the derivation of a singular value decomposition. Regarding the Radon transform $\mathcal{R}$ for instance, the singular value decomposition is known if $\mathcal{R}$ is considered as mapping $L_2(V_1(0)) \to L_2([0, 2\pi] \times [-1, 1], w)$ with weight $w(s) := (1 - s^2)^{-1/2}$.

In case of a moderate deformation, the dynamic forward operator $\mathcal{A}_\Gamma$ is given by $\mathcal{A}_\Gamma = \mathcal{V}\mathcal{A}$ with an operator $\mathcal{V}$ as stated in (9). We start by summarizing properties of this mapping $\mathcal{V}$ from [16].

Theorem 1 *The operator*

$$\mathcal{V} : L_2([0, T] \times \Omega_Y, w) \longrightarrow L_2(M([0, T] \times \mathbb{R}^m), w_\Gamma)$$

$$\mathcal{V}g(t, y) = \alpha(t, y)\, g(M(t, y))$$

with weight $w_\Gamma(t, y) = |\det DM(t, y)|\, \alpha(t, y)^{-2}\, w(M(t, y))$ is linear and bijective with inverse

$$\mathcal{V}^{-1} = \mathcal{V}^*.$$

Proof According to its Definition, $\mathcal{V}$ is linear. We first compute its adjoint

$$\mathcal{V}^* : L_2(M([0, T] \times \Omega_Y), w_\Gamma) \longrightarrow L_2([0, T] \times \Omega_Y, w).$$

It holds

$$\langle \mathcal{V}g, h \rangle_{L_2([0,T] \times \Omega_Y, w_\Gamma)} = \int_{[0,T] \times \Omega_Y} \mathcal{V}g(t, y)\, h(t, y)\, w_\Gamma(t, y)\, \mathrm{d}t\mathrm{d}y$$

$$= \int_{[0,T]\times\Omega_Y} \alpha(t, y)^{-1} g(M(t, y)) h(t, y) \, | \det DM(t, y)| \, w(M(t, y)) \, \mathrm{d}t \mathrm{d}y$$

$$= \int_{M([0,T]\times\Omega_Y)} g(t, y) \, m\left(M^{-1}(t, y)\right)^{-1} h(M^{-1}(t, y)) \, w(t, y) \, \mathrm{d}t \mathrm{d}y$$

$$= \langle g, \mathcal{V}^* h \rangle_{L_2(M([0,T]\times\Omega_Y), w)}$$

with $\mathcal{V}^* h(t, y) = m\left(M^{-1}(t, y)\right)^{-1} h(M^{-1}(t, y))$. For $g \in L_2([0, T] \times \Omega_Y, w)$, we further obtain

$$\mathcal{V}^* \mathcal{V} g(t, y) = m\left(M^{-1}(t, y)\right)^{-1} \mathcal{V} g(M^{-1}(t, y))$$

$$= m\left(M^{-1}(t, y)\right)^{-1} m\left(M^{-1}(t, y)\right) g(M(M^{-1}(t, y)))$$

$$= g(t, y),$$

and respectively for $g \in L_2(M([0, T] \times \Omega_Y), w_\Gamma)$

$$\mathcal{V} \mathcal{V}^* g(t, y) = g(t, y),$$

i.e. $\mathcal{V}^{-1} = \mathcal{V}^*$.   □

Due to the properties of $\mathcal{V}$ verified in Theorem 1, many properties of the static operator $\mathcal{A}$ transfer directly to its dynamic counterpart $\mathcal{A}_\Gamma$. A detailed overview is given in [16]. The following Lemma states some of these properties which are relevant regarding the formulation of suitable dynamic regularization methods.

Lemma 1

(i) If $\mathcal{A} : L_2(\Omega_X) \to L_2([0, T] \times \Omega_Y, w)$ is continuous, then

$$\mathcal{A}_\Gamma : L_2(\Omega_X) \to L_2(M([0, T] \times \Omega_Y), w_\Gamma)$$

is continuous.

(ii) Regarding the nullspace, noted N, it holds

$$N(\mathcal{A}_\Gamma) = N(\mathcal{A}). \tag{13}$$

(iii) Let $\mathcal{A}^\dagger$ be the generalized inverse of $\mathcal{A}$. Then, the pseudoinverse of $\mathcal{A}_\Gamma$ is given by

$$\mathcal{A}_\Gamma^\dagger = \mathcal{A}^\dagger \mathcal{V}^{-1}.$$

Proof

(i) Since $\mathcal{V}$ is a unitary transformation, it holds

$$\|\mathcal{A}_\Gamma\|_{L_2(M([0,T]\times\Omega_Y),w_\Gamma)} = \|\mathcal{A}\|_{L_2([0,T]\times\Omega_Y,w)}.$$

(ii) The nullspace property follows from the bijectivity of $\mathcal{V}$.

(iii) Let $f = \mathcal{A}_\Gamma^\dagger g$, i.e. $f \in N(\mathcal{A}_\Gamma)^\perp$ and $\mathcal{A}_\Gamma^* \mathcal{A}_\Gamma f = \mathcal{A}_\Gamma^* g$. Since $\mathcal{V}$ is a unitary operator, it holds

$$\mathcal{A}_\Gamma^* \mathcal{A}_\Gamma = \mathcal{A}^* \mathcal{V}^* \mathcal{V} \mathcal{A} = \mathcal{A}^* \mathcal{A},$$

and further

$$\mathcal{A}^* \mathcal{A} f = \mathcal{A}^* \mathcal{V}^{-1} g.$$

Due to the nullspace property (13), $f \in N(\mathcal{A}_\Gamma)^\perp$ implies $f \in N(\mathcal{A})^\perp$. Thus, $f = \mathcal{A}^\dagger \mathcal{V}^{-1} g$.

□

From the proof of Lemma 1 iii), it follows directly for the domain $\mathcal{D}(\mathcal{A}_\Gamma^\dagger) = R(\mathcal{A}_\Gamma) \oplus R(\mathcal{A}_\Gamma)^\perp$, where $R(\mathcal{A}_\Gamma)$ denotes the range of $\mathcal{A}_\Gamma$:

Corollary 1 *For $g \in \mathcal{D}(\mathcal{A}_\Gamma^\dagger)$, it holds $\mathcal{V}^{-1} g \in \mathcal{D}(\mathcal{A}^\dagger)$.*

With these properties, we can show the following regularization property.

Theorem 2 *Let the family $(\mathcal{T}_\gamma)_{\gamma\in(0,\infty)}$ be a regularization for $\mathcal{A}^\dagger$. Then, the family $(\mathcal{S}_\gamma)_{\gamma\in(0,\infty)}$ with*

$$\mathcal{S}_\gamma := \mathcal{T}_\gamma \mathcal{V}^{-1}$$

is a regularization for $\mathcal{A}_\Gamma^\dagger$.

Proof Let $g \in \mathcal{D}(\mathcal{A}_\Gamma^\dagger)$ and $\|g - g^\epsilon\| \le \epsilon$. With Corollary 1, it follows $\mathcal{V}^{-1} g \in \mathcal{D}(\mathcal{A}^\dagger)$ and due to the unitary property of $\mathcal{V}$, it holds $\|\mathcal{V}^{-1} g - \mathcal{V}^{-1} g^\epsilon\| = \|g - g^\epsilon\| \le \epsilon$. Since $(\mathcal{T}_\gamma)_{\gamma\in(0,\infty)}$ is a regularization for $\mathcal{A}^\dagger$, we obtain with the parameter choice rule $\gamma = \gamma(\epsilon, g^\epsilon)$ and the regularizing property of $(T_\gamma)_{\gamma\in(0,\infty)}$

$$\lim_{\substack{\epsilon\to 0 \\ g^\epsilon\to g}} \mathcal{S}_{\gamma(\epsilon,g^\epsilon)} g^\epsilon = \lim_{\substack{\epsilon\to 0 \\ g^\epsilon\to g}} \mathcal{T}_{\gamma(\epsilon,g^\epsilon)} \mathcal{V}^{-1} g^\epsilon = \mathcal{A}^\dagger \mathcal{V}^{-1} g = \mathcal{A}_\Gamma^\dagger g.$$

This concludes the proof.

□

Thus, for moderate deformations, we obtain a dynamic regularization method for solving $\mathcal{A}_\Gamma f_0 = g$ by adapting any static regularization for $\mathcal{A}$ according to the transform $\mathcal{V}$.

Further properties, including a singular value decomposition and a characterization of the ill-posedness of the dynamic forward operator $\mathcal{A}_\Gamma$ under moderate deformation Γ can be found in [16].

Example: Photoacoustic Tomography

To illustrate the theoretical results of this section, we consider the static inverse problem $\mathcal{A}f = g$ with the circular Radon transform

$$\mathcal{A}f(\theta(t), r) = \frac{1}{2\pi r} \int_{V_1(0)} f(x)\, \delta(r - \|\theta(t) - x\|)\, dx, \qquad (14)$$

which integrates a measurable function f supported inside the unit disk $V_1(0) \subset \mathbb{R}^2$ along circles

$$C(t, r) = \{x \in \mathbb{R}^2 \, : \, \|x - \theta(t)\| = r\}$$

with $\theta(t) = (\cos(t), \sin(t))^T$ and $(t, r) \in [0, 2\pi] \times (0, \infty)$. This operator represents for instance a simplified mathematical model in 2D photoacoustic tomography (PAT), see for instance [26].

Theorem 3 *Let $(\Gamma_t)_{t \in [0,T]}$ describe a rotational movement of the initial state f_0, i.e. $\Gamma_t x := A_t x$ with unitary matrix*

$$A_t = \begin{pmatrix} \cos(\omega_t) & -\sin(\omega_t) \\ \sin(\omega_t) & \cos(\omega_t) \end{pmatrix} \in \mathbb{R}^{2 \times 2}$$

for all $t \in [0, 2\pi]$ with $\omega_t \in \mathbb{R}$ such that $\{\theta(t + \omega_t) \, : \, t \in [0, 2\pi]\} = S^1$. Then, the dynamic operator $\mathcal{A}_\Gamma$ is related to the static transform $\mathcal{A}$ via

$$\mathcal{A}_\Gamma = \mathcal{V}\mathcal{A}$$

with $\mathcal{V}g(\theta_t, r) = g(\theta_{\omega_t + t}, r)$.

Thus, rotations as stated in the Theorem are moderate deformations with respect to the spherical Radon transform.

Proof According to (7), the dynamic operator $\mathcal{A}_\Gamma$ with the stated motion model is given by

$$\mathcal{A}_\Gamma f(t, r) = \frac{1}{2\pi r} \int_{V_1(0)} |\det A_t^{-1}|\, f(x)\, \delta(r - \|\theta(t) - A_t^{-1}x\|)\, dx.$$

For each $t \in [0, 2\pi]$, A_t represents a rotation with angle ω_t, i.e. it holds $|\det A_t^{-1}| = 1$, and we further obtain

$$\mathcal{A}_\Gamma f(\theta(t), r) = \frac{1}{2\pi r} \int_{V_1(0)} f(x)\, \delta(r - \|A_t \theta(t) - x\|)\, dx$$

$$= \mathcal{V} \mathcal{A}_\Gamma(\theta(t), r)$$

with $\mathcal{V}g(\theta(t), r) = g(\theta(\omega_t + t), r)$.   □

Remark 2

(i) Please note that the property $\{\theta(t + \omega_t) : t \in [0, 2\pi]\} = S^1$ guarantees the required diffeomorphism property of the transform $T : S^1 \times (0, \infty) \longrightarrow S^1 \times (0, \infty)$. Descriptively, this condition ensures that all information about the object f are actually encoded in the dynamic data $g = \mathcal{A}_\Gamma f$. This is studied in more detail in the subsequent book chapter *Microlocal properties of dynamic Fourier integral operators*.

(ii) Theorem 3 states, that in the presence of an object rotation, the dynamic operator $\mathcal{A}_\Gamma$ still integrates along circles. The additional constraint on the rotation sequence $(A_t)_{t \in [0, 2\pi]}$ ensures, that all these modified circles cover the complete unit disk (i.e. the support of the object).

Theorem 4 *A suitable reconstruction method* $\mathcal{S}^{\mathrm{DFBP}} : L_2(S^1 \times (0, 2)) \rightarrow L_2(V_1(0))$ *for dynamic photoacoustic tomography with rotational movement as stated above is given by*

$$\mathcal{S}^{\mathrm{DFBP}} g(x) = \frac{1}{2\pi} \int_0^{2\pi} \int_0^2 (\partial_r r \partial_r g)(\theta(t), r) \, \log \left| r^2 - \|x - \Gamma_t \theta(t)\|^2 \right| \, dr\, dt.$$

Proof Since rotational deformations as stated above are moderate deformations with respect to the circular Radon transform, we obtain a suitable dynamic reconstruction method by adapting an established regularization strategy from the static case. The circular Radon transform as given in (14) is well known in the literature and various inversion formulae were worked out, for instance in the 2D case as

$$f(x) = \frac{1}{2\pi} \int_0^{2\pi} \int_0^2 (\partial_r r \partial_r \mathcal{A} f)(\theta(t), r) \, \log \left| r^2 - \|x - \theta(t)\|^2 \right| \, dr\, dt$$

$$=: \mathcal{T}^{FBP} f(x),$$

(continued)

see [11], providing a static reconstruction method denoted $\mathcal{T}^{FBP}$. Thus, $\mathcal{S}^{DFBP} := \mathcal{T}^{FBP}\mathcal{V}^{-1}$ is a dynamic reconstruction method according to Theorem 2 and with the representation of $\mathcal{V}$, it holds

$$
\begin{aligned}
\mathcal{S}^{DFBP} g(x) &= \frac{1}{2\pi} \int_0^{2\pi} \int_0^2 (\partial_r r \partial_r \mathcal{V}^{-1} g)(\theta(t), r) \, \log \left| r^2 - \|x - \theta(t)\|^2 \right| \, \mathrm{d}r \mathrm{d}t \\
&= \frac{1}{2\pi} \int_0^{2\pi} \int_0^2 \mathcal{V}^{-1}(\partial_r r \partial_r g)(\theta(t), r) \, \log \left| r^2 - \|x - \theta(t)\|^2 \right| \, \mathrm{d}r \mathrm{d}t \\
&= \frac{1}{2\pi} \int_0^{2\pi} \int_0^2 (\partial_r r \partial_r g)(\theta(t), r) \, \log \left| r^2 - \|x - A_t \theta(t)\|^2 \right| \, \mathrm{d}r \mathrm{d}t.
\end{aligned}
$$

This concludes the proof.   □

For the numerical evaluation, we consider the phantom depicted in Fig. 4 (left). In this example, the phantom performs on the time interval $[0, \pi]$ a rotational movement given by the angles $\omega_t = t/10$, $t \in [0, \pi]$ and during $[\pi, 2\pi]$ returns to its initial state. The state of the object at the end of the scanning is shown in Fig. 4 (right).

The respective PAT data are simulated by discretizing the forward operator $\mathcal{A}_\Gamma$ with the trapezoidal rule with 1400 samples. More precisely, we hereby obtain the discrete data

$$
g_{j,k} := (\mathcal{A}_{\Gamma_{t_j}} f)(t_j, r_k), \quad j = 1, \ldots, N \text{ and } k = 1, \ldots, M,
$$

where t_j are uniformly distributed angles in $[0, 2\pi)$, r_k uniformly distributed in $[0, 2]$ with $N = 300$, $M = 300$. Furthermore, in order to test stability, we add a sample of White Noise to the data set, corresponding to a noise level of 2.5%.

The result of the above stated reconstruction method is illustrated in Fig. 5 (left), which shows the reconstructed initial state of the object on a 512×512 grid. Figure 5 (right) illustrates the result of the static filtered backprojection algorithm applied to the dynamic data. The comparison with the exact initial state shows that the dynamic reconstruction technique in fact compensates for the motion while the static algorithm causes strong distortion artefacts.

Further examples, including a detailed evaluation regarding computerized tomography can be found in [16].

Fig. 4 Phantom at the initial time $t = 0$ (left) and at half time of the scanning, i.e. at time $t = \pi$ (right)
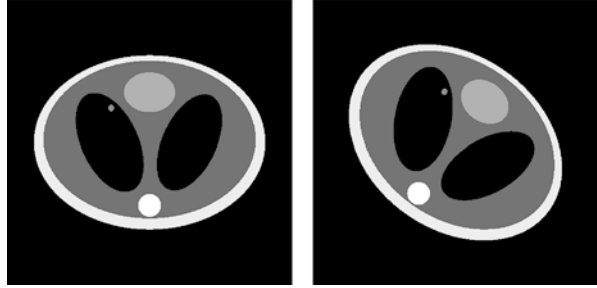
Fig. 5 Dynamic reconstruction at the initial time (left) and static reconstruction (right) from noisy data
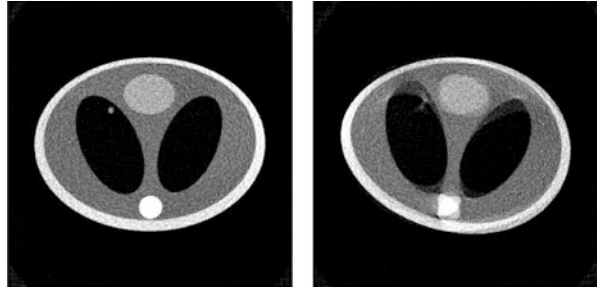
4   Compensating General Deformations via the Method of the Approximate Inverse

After working out a regularization theory for moderate deformations, we now turn towards the more general scenario of strong deformations. To this purpose, we focus on (8) and apply the method of the approximate inverse which calculates linear functionals of the sought-for solution, see [30, 32]. To simplify the notation, we consider in the following

$$\mathcal{A} : L_2(\Omega_X) \rightarrow L_2([0, T] \times \Omega_Y),$$

i.e. as mapping between classical L_2-spaces. Nevertheless, the presented theory can be easily extended to weighted L_2-spaces as well.

4.1   The Method of the Approximate Inverse

In order to obtain a stable approximation of the solution f_0, we calculate the smoothed version f_0^γ,

$$f_0(x) \approx f_0^\gamma(x) = \langle f_0, \delta_x^\gamma \rangle_{L_2(\Omega_X)}$$

with a prescribed *mollifier* δ_x^γ. The precise definition of a mollifier is given in the following, see also [46].

Definition 1 For all $x \in \Omega_X$, let $\delta_x^\gamma \in L_2(\Omega_X)$ with

$$\int_{\Omega_X} \delta_x^\gamma(z)\, dz = 1, \quad \gamma > 0.$$

Let further

$$f^\gamma(x) = \int_{\Omega_X} f(z)\, \delta_x^\gamma(z)\, dz$$

converge to f in $L_2(\Omega_X)$ as $\gamma \to 0$. Then, δ_x^γ is called a mollifier.

A mollified version f_0^γ can be reconstructed by evaluating linear functionals on the measured dynamic data $g = \mathcal{A}_\Gamma f_0$.

Theorem 5 *Let $\delta_x^\gamma \in L_2(\Omega_X)$ be a mollifier and let ψ_x^γ be the solution of*

$$\mathcal{A}_\Gamma^* \psi_x^\gamma = \delta_x^\gamma. \tag{15}$$

Then,

$$f_0^\gamma(x) = \langle g, \psi_x^\gamma \rangle_{L_2([0,T] \times \Omega_Y)}.$$

Equation (15) is called *auxiliary problem*, its solution ψ_x^γ called *reconstruction kernel*. Since $\mathcal{A}_\Gamma$ depends on the dynamic behavior, we speak of Eq. (15) as *dynamic auxiliary problem*, and of ψ_x^γ as *dynamic reconstruction kernel*.

As a further specification, we call ψ_x^γ a *special reconstruction kernel* since it depends on the specific reconstruction point x.

The Approximate Inverse

Theorem 5 introduces an operator $\mathcal{S}^\gamma : L_2([0,T] \times \Omega_Y) \to L_2(\Omega_X)$ with $\mathcal{S}^\gamma g(x) = \langle g, \psi_x^\gamma \rangle_{L_2}$, which is called *approximate inverse* of $\mathcal{A}_\Gamma$. The regularization property of the method is ensured by imposing conditions on the mollifier and on the choice of parameter γ [30, 31]. The effect of the dynamic behavior on the smoothing properties of the forward operator is analyzed in the chapter *Microlocal properties of dynamic Fourier integral operators* [19].

Since the auxiliary problem (15) is independent of the data, the reconstruction kernel ψ_x^γ can be precomputed. In principle, mollifiers for different reconstruction points x can be chosen independently. In this case, however, the auxiliary problem

(15) has to be solved for distinct right-hand sides leading to high computational costs and storage needs. This effort can be reduced by considering invariances of $\mathcal{A}_\Gamma^*$.

Theorem 6 *Let*

$$T_1^x : L_2(\Omega_X) \to L_2(\mathbb{R}^n), \quad T_2^x : L_2([0, T] \times \Omega_Y) \to L_2([0, T] \times \mathbb{R}^m)$$

be linear operators with

$$T_1^x \mathcal{A}_\Gamma^* = \mathcal{A}_\Gamma^* T_2^x, \tag{16}$$

and let ψ^γ be a solution of the auxiliary problem

$$\mathcal{A}_\Gamma^* \psi^\gamma = \delta^\gamma \tag{17}$$

with $\delta^\gamma \in L_2(\Omega_X)$. Then a solution of

$$\mathcal{A}_\Gamma^* \psi_x^\gamma = \delta_x^\gamma$$

with the special mollifier

$$\delta_x^\gamma = T_1^x \delta^\gamma \tag{18}$$

is given by

$$\psi_x^\gamma = T_2^x \psi^\gamma.$$

Proof According to the relations (16), (17), and (18), it holds

$$\mathcal{A}_\Gamma^* T_2^x \psi^\gamma = T_1^x \mathcal{A}_\Gamma^* \psi^\gamma = T_1^x \delta^\gamma = \delta_x^\gamma,$$

and thus, $T_2^x \psi_\gamma$ solves the auxiliary problem $\mathcal{A}_\Gamma^* \psi_x^\gamma = \delta_x^\gamma$.   □

Consequently, only a single auxiliary problem has to be solved while the special mollifiers and corresponding reconstruction kernels are generated by applying the operators T_1^x and T_2^x, respectively.

Remark 3 The method of the approximate inverse can be extended to enable the so-called *feature reconstruction*, where a feature $\mathcal{L} f_0$ with a linear feature operator $\mathcal{L}$ is determined directly from the measured data, see [20, 31]. In this case, the respective reconstruction kernel can be computed by solving the auxiliary problem

$$\mathcal{A}_\Gamma^* \psi_x^\gamma = \mathcal{L}^* \delta_x^\gamma,$$

and efficient algorithms are obtained by considering linear invariance properties for $\mathcal{A}_\Gamma^*$ as well as $\mathcal{L}^*$.

4.2 Computing the Dynamic Reconstruction Kernel

We now address the solution of the auxiliary problem (15). In static CT, for instance, an explicit representation of the kernel ψ^γ can be derived using the inversion formula for the Radon transform [31]. For dynamic forward operators $\mathcal{A}_\Gamma$, no general inversion formula is known so far. Thus, we present an alternative strategy to compute suitable dynamic reconstruction kernels. The idea consists in exploiting the relation with the time-resolved forward operator $\mathcal{A}^{dyn}$ and its adjoint operator.

$$\mathcal{A}^{dyn*}g(t, x) = \int_{\mathbb{R}^m} \overline{k(x, t, y)}\, g(t, y)\, \mathrm{d}y.$$

Theorem 7 *Let δ_x^γ be a mollifier for the initial state function f_0 and denote*

$$e_{0,x}^\gamma(t, z) = \left(\int_{[0,T]} |\det D\Gamma_v^{-1}(\Gamma_t z)|\, \mathrm{d}v \right)^{-1} \delta_x^\gamma(\Gamma_t z). \tag{19}$$

Further assume there exists $\psi_{0,x}^\gamma$ with

$$\mathcal{A}^* \psi_{0,x}^\gamma = e_{0,x}^\gamma. \tag{20}$$

Then, it holds

(i)

$$\langle f, e_{0,x}^\gamma \rangle_{L_2([0,T]\times\Omega_X)} = \langle f_0, \delta_{0,x}^\gamma \rangle_{L_2(\Omega_X)},$$

in particular, $e_{0,x}^\gamma$ is a time-dependent mollifier incorporating the motion information,

(ii)

$$\mathcal{A}^{dyn*}_\Gamma \psi_{0,x}^\gamma = \delta_x^\gamma,$$

i.e. $\psi_{0,x}^\gamma$ is our searched-for reconstruction kernel.

Proof

(i) From the definition of $e_{0,x}^\gamma$, it follows

$$\int_{[0,T]} |\det D\Gamma_t^{-1} z| \, e_{0,x}^{\gamma}(t, \Gamma_t^{-1} z) \, dt$$

$$= \int_{[0,T]} |\det D\Gamma_t^{-1} z| \, \delta_x^{\gamma}(z) \left(\int_{[0,T]} |\det D\Gamma_v^{-1}(z)| \, dv \right)^{-1} dt = \delta_x^{\gamma}(z).$$

Together with the temporal correlation (1), namely $f(t, x) = f_0(\Gamma_t x)$, the support property (2) and the substitution $\overline{z} := \Gamma_t(z)$, we then obtain

$$\langle f, e_{0,x}^{\gamma} \rangle_{L_2([0,T] \times \Omega_X)} = \int_{[0,T] \times \Omega_X} f(t, z) \, e_{0,x}^{\gamma}(t, z) \, dt \, dz$$

$$= \int_{[0,T] \times \mathbb{R}^n} f_0(\Gamma_t z) \, e_{0,x}^{\gamma}(t, z) \, dt \, dz$$

$$= \int_{[0,T] \times \mathbb{R}^n} f_0(\overline{z}) \, |\det D\Gamma_t^{-1} \overline{z}| \, e_{0,x}^{\gamma}(t, \Gamma_t^{-1} \overline{z}) \, dt \, d\overline{z}$$

$$= \int_{\mathbb{R}^n} f_0(z) \, \delta_x^{\gamma}(\overline{z}) \, dt \, d\overline{z}$$

$$= \langle f_0, \delta_x^{\gamma} \rangle_{L_2(\Omega_X)}.$$

A simple calculation further shows

$$\int_{[0,T] \times \mathbb{R}^n} e_{0,x}^{\gamma}(v, z) \, dv \, dz = \int_{\mathbb{R}^n} \delta_x^{\gamma}(z) \, dz = 1,$$

i.e. $e_{0,x}^{\gamma}$ is in fact a time-dependent mollifier for $f(0, x)$ according to Definition 1.

(ii) The correlation between δ_x^{γ} and $e_{0,x}^{\gamma}$ from the proof of i) along with the equation $\mathcal{A}^{dyn*} \psi_{0,x}^{\gamma} = e_{0,x}^{\gamma}$ and the representations of $\mathcal{A}^{dyn*}$ and $\mathcal{A}_{\Gamma}^{*}$, see (11) and (12), yields

$$\delta_x^{\gamma}(z) = \int_{[0,T]} |\det D\Gamma_t^{-1} z| \, e_{0,x}^{\gamma}(t, \Gamma_t^{-1} z) \, dt$$

$$= \int_{[0,T]} |\det D\Gamma_t^{-1} z| \, \mathcal{A}^{dyn*} \psi_{0,x}^{\gamma}(t, \Gamma_t^{-1} z) \, dt$$

$$= \int_{[0,T]} |\det D\Gamma_t^{-1} z| \, \mathcal{A}_t^{*} \psi_{0,x}^{\gamma}(t, \Gamma_t^{-1} z) \, dt$$

$$= \mathcal{A}_{\Gamma}^{*} \psi_{0,x}^{\gamma}(z).$$

Thus, $\psi_{0,x}^{\gamma}$ is the searched-for dynamic reconstruction kernel.

$\square$

Exploiting invariances, it is sufficient to solve the auxiliary problem for $x = 0$, i.e. $\mathcal{A}^{dyn*}\psi^\gamma = e^\gamma$ with $e^\gamma := e_{0,0}^\gamma$.

What if e^γ Is Not in the Range of $\mathcal{A}^*$?

If e^γ is not in the range of $\mathcal{A}^*$, then the auxiliary problem $\mathcal{A}^*\psi^\gamma = e^\gamma$ has no solution in the classical sense and instead, the generalized solution via the Moore-Penrose inverse has to be computed. However, an analysis provided in [15] turns out, that in the static setting, the generalized solution of (20) does not represent an adequate approximation to the exact kernel. Thus, [15] proposed instead to approximate ψ^γ by minimizing the penalized defect

$$\left\| \mathcal{A}^{dyn*}\psi^\gamma - e^\gamma \right\|^2 + \alpha \left\| \psi^\gamma - \psi^{\gamma,stat} \right\|^2, \quad \alpha > 0,$$

or equivalently by solving the normal equation

$$(\mathcal{A}^{dyn}\mathcal{A}^{dyn*} + \alpha I)\psi^\gamma = \mathcal{A}^{dyn}e^\gamma + \alpha\psi^{\gamma,stat}$$

with the identity operator I, incorporating the exact static reconstruction kernel in the penalty term. The numerical examples in [15] as well as our results in Sect. 4.3 will illustrate that reconstruction kernels of this kind provide in fact a good motion compensation. Besides, the normal equation is an integral equation of the second kind, so it can be solved numerically without the severe problems arising for equations of the first kind.

We now address suitable invariance operators for the dynamic scenario. This is studied in detail in [15].

For affine deformations, we can adapt invariances holding in the static case to invariance properties in the dynamic case.

Theorem 8 *Let* $T_1^x : L_2(\Omega_X) \longrightarrow L_2(\mathbb{R}^n)$ *and* $T_2^{x,t} : L_2(\Omega_Y) \longrightarrow L_2(\mathbb{R}^m)$ *be invariance operators for the static problem with fixed time instance t, i.e.*

$$T_1^x \mathcal{A}_t^* = \mathcal{A}_t^* T_2^{x,t} \quad \forall\, x, t.$$

Then, for affine motion functions Γ_t, $t \in [0, T]$, *it holds*

$$T_1^x \mathcal{A}_\Gamma^* = \mathcal{A}_\Gamma^* T_2^{dyn}$$

with

$$T_2^{dyn} : L_2([0, T] \times \mathbb{R}^m) \longrightarrow L_2([0, T] \times \mathbb{R}^m)$$

$$T_2^{dyn} g(t, y) := T_2^{\Gamma_t^{-1}x - \Gamma_t^{-1}0, t} g_t(y).$$

Proof Since Γ_t is an affine mapping, it holds in particular

$$\Gamma_t^{-1}(z - x) = \Gamma_t^{-1}z - (\Gamma_t^{-1}x - \Gamma_t^{-1}(0)).$$

With the definition of the involved operators, we obtain

$$\mathcal{A}_\Gamma^* T_2^{dyn} g(z) = \int_{[0,T]} |\det D\Gamma_t^{-1}z| \, \mathcal{A}_t^* T_2^{\Gamma_t^{-1}x - \Gamma_t^{-1}0, t} g_t(\Gamma_t^{-1}x) \, \mathrm{d}t$$

$$= \int_{[0,T]} |\det D\Gamma_t^{-1}z| \, T_1^{\Gamma_t^{-1}x - \Gamma_t^{-1}0} \mathcal{A}_t^* g_t(\Gamma_t^{-1}z) \, \mathrm{d}t$$

$$= \int_{[0,T]} |\det D\Gamma_t^{-1}z| \, \mathcal{A}_t^* g_t(\Gamma_t^{-1}z - (\Gamma_t^{-1}x - \Gamma_t^{-1}0)) \, \mathrm{d}t$$

$$= \int_{[0,T]} |\det D\Gamma_t^{-1}z| \, \mathcal{A}_t^* g_t(\Gamma_t^{-1}(z - x)) \, \mathrm{d}t$$

$$= \mathcal{A}_\Gamma^* g(z - x)$$

$$= T_1^x \mathcal{A}_\Gamma^* g(z).$$

This concludes the proof.   □

Remark 4 As discussed in [15], deriving linear invariances in the presence of non-linear object motion might in general not be possible. Hence, the use of approximate invariances is suggested instead and an error analysis has been provided. For our numerical examples, we are going to use approximate invariance which are exact for affine deformations, namely by using the operators T_1^x and T_2^{dyn} as defined above.

4.3 Applications

We want to illustrate our general dynamic reconstruction technique at the example of 3D X-ray tomography. An evaluation regarding 2D computerized tomography with parallel scanning geometry can be found in [15].

Example: 3D X-Ray Tomography
We consider an X-ray source emitting a cone of X-rays through the studied specimen to a 2D detector. The movement of the combination source-detector determines different geometries. Let $M \subset \mathbb{R}^3$ describe the curve of the X-ray

source. Then, the mathematical model of 3D-CT for a static object h is given by the cone-beam transform

$$\mathcal{D}h(a, \theta) = \int_0^\infty h(a + \beta\theta)\,\mathrm{d}\beta$$

with $a \in M \subset \mathbb{R}^3$ denoting the position of the source and $\theta \in S^2$ characterizing the direction of the ray.

One simple realization consists in rotating the radiation source on a circle around the specimen with radius $R > 0$, i.e. $M = \{R(\cos(\varphi), \sin(\varphi), 0)^T \mid \varphi \in [0, 2\pi]\}$. Despite some drawbacks from a mathematical point of view (for instance the Tuy–Kirillov condition is not satisfied resulting in incomplete data), this geometry is used in many real-world applications. Thus, we consider this setting in the following.

As in the 2D case, see the example of the Radon transform on page 7, the rotation of the radiation source represents the time-dependent step of the data acquisition, i.e. we identify the angle φ which characterizes the current source position as time variable. Thus, we obtain the dynamic operator

$$\mathcal{D}^{dyn} f(t, \theta) = \int_0^\infty f(a(t) + \beta\theta, t)\,\mathrm{d}\beta$$

for a time-dependent function $f \in L_2([0, T] \times \Omega_X)$. If we further incorporate the motion information, we obtain

$$\mathcal{D}_\Gamma f_0(t, \theta) = \int_0^\infty f_0(\Gamma_t(a(t) + \beta\theta))\,\mathrm{d}\beta$$

as dynamic operator for the initial state f_0, respectively.

In order to derive a reconstruction algorithm which compensates for the motion, we apply the method proposed in Sect. 4.2. Following Theorem 7, we determine the reconstruction kernel ψ^γ by considering the auxiliary problem

$$\mathcal{D}^{dyn*}\psi^\gamma = e^\gamma, \tag{21}$$

with the time-dependent mollifier e^γ (19) stemming from the static mollifier δ^γ.

Lemma 2 *The adjoint operator $\mathcal{D}^{dyn*}$ as mapping from $L_2([0, 2\pi] \times S^2)$ to $L_2([0, 2\pi] \times \mathbb{R}^3)$ is given by*

$$\mathcal{D}^{dyn*} g(t, x) = \|x - a(t)\|^{-2} g\left(a(t), \frac{x - a(t)}{\|x - a(t)\|}\right).$$

Proof Since the investigated object has compact support (and is surrounded by source and detector), there is a minimal radius L such that $\operatorname{supp} f \subset V_L(0)$ and $L < R$. Therefore, in the definition of the cone beam transform, we can restrict ourselves to the integration over a compact interval $[L_1, L_2] \subset \mathbb{R}$, where $0 < L_1 < R - L$ and $L_2 > L + R$. This results in the following representation for the dynamic operator

$$\mathcal{D}^{dyn} f(t, \theta) = \int_{L_1}^{L_2} f(a(t) + \beta\theta, t) \, d\beta.$$

With the substitution $x := a(t) + \beta\theta$, we obtain

$$\langle \mathcal{D}^{dyn} f, g \rangle_{L_2([0,2\pi] \times S^2)} = \int_{[0,2\pi]} \int_{S^2} \int_{L_1}^{L_2} f(a(t) + \beta\theta, t) \, g(t, \theta) \, d\beta \, d\theta \, dt$$

$$= \int_{[0,2\pi]} \int_{V_L(0)} f(x, t) \, \|x - a(t)\|^{-2}$$

$$g\left(t, \frac{x - a(t)}{\|x - a(t)\|}\right) dx \, dt,$$

and thus the stated representation for $\mathcal{D}^{dyn*}$.   □

A generalized solution of (21) is computed via the penalized normal equation

$$(\mathcal{D}^{dyn} \mathcal{D}^{dyn*} + \alpha I)\psi^\gamma = \mathcal{D}^{dyn} e^\gamma + \alpha \psi^{\gamma,stat}.$$

Due to the property

$$\mathcal{D}^{dyn} \mathcal{D}^{dyn*} g(t, \theta) = \int_{L_1}^{L_2} \mathcal{D}^{dyn*} g(a(t) + \beta\theta, t) \, d\beta$$

$$= \int_{L_1}^{L_2} \|\beta\theta\|^{-2} g\left(t, \frac{\beta\theta}{\|\beta\theta\|}\right) d\beta$$

$$= \left(\frac{1}{L_1} - \frac{1}{L_2}\right) g(t, \theta),$$

with appropriately selected $L_1, L_2 \in \mathbb{R}$ (see proof of Lemma 2), we obtain

$$\psi^\gamma = \left(\frac{1}{L_1} - \frac{1}{L_2} + \alpha\right)^{-1} \left(\mathcal{D}^{dyn} e^\gamma + \alpha \psi^{\gamma,stat}\right).$$

Thus, the reconstruction kernel for dynamic cone-beam tomography results from averaging the generalized solution of the dynamic auxiliary problem and the static reconstruction kernel. In the static case, suitable reconstruction kernels have been derived for the circular cone beam transform. For instance, the static reconstruction kernel associated to the Gaussian mollifier

$$\delta^\gamma (z) = (2\pi)^{-3/2} \frac{1}{\gamma^3} e^{-\frac{\|z\|^2}{2\gamma^2}}$$

has been computed by Weber in his PhD-thesis [49] and in [33]. Further, he and his co-authors derived the special reconstruction kernels $\psi_x^{\gamma, stat}$ by

$$\psi_x^{\gamma, stat} (a(t), \theta) = T_2^{x,t} \psi^\gamma (a(t), \theta)$$

with (approximate) invariance operator

$$T_2^{x,t} \psi (a(t), \theta) = \frac{R^2}{\|a - x\|^2} \psi (a, U_x^T \theta),$$

where U_x^T corresponds to the unitary matrix that rotates $\frac{a-x}{\|a-x\|}$ onto a/R, i.e.

$$U_x^T \frac{a - x}{\|a - x\|} = \frac{a}{R}.$$

We adapt this invariance operator according to Theorem 8 and Remark 4 to the dynamic setting with motion model Γ.

Numerical Results

The algorithm is tested for the three-dimensional phantom with compact support in $V_1(0)$ whose initial state is shown in Fig. 6 (first row) for three different cross sections throughout the object. The dynamic behavior is described by the nonlinear scaling

$$\Gamma_t x = \begin{pmatrix} \frac{(s_1(t) x_1 + 1)^5 - 1}{5 s_1(t)} \\ \frac{(s_2(t) x_2 + 1)^5 - 1}{5 s_2(t)} \\ \frac{x_3}{s_3(t)} \end{pmatrix}$$

with
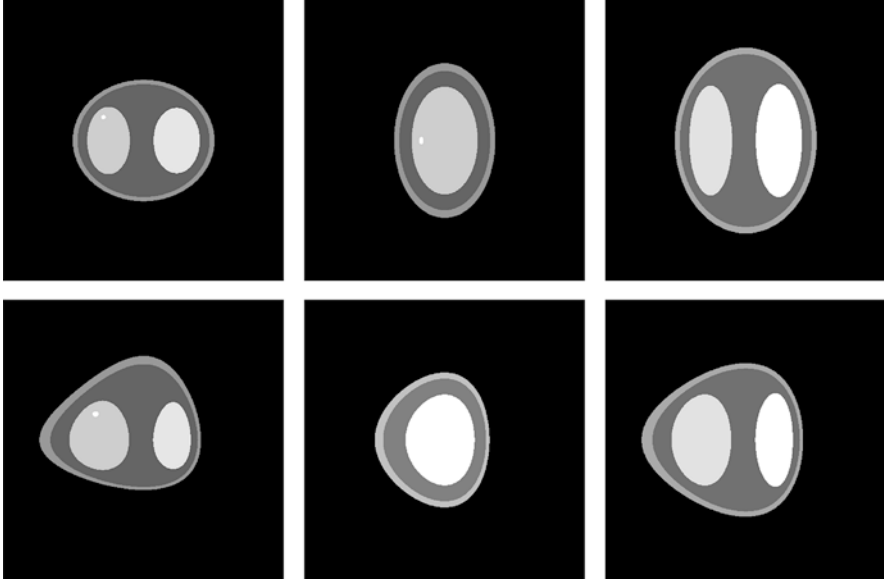
Fig. 6 Initial state (first row) and final state (second row) of our 3D phantom with nonaffine deformation. The three columns correspond to different crossections of the phantom (first column: fixed component $x_3 = 0$, second column: fixed component $x_2 = -0.27$, third column: fixed component $x_1 = 0$)

$$s_1(t) = \sqrt[4]{\sin(0.0375 \cdot t/\pi)}, \quad s_2(t) = \sqrt[4]{\sin(0.045 \cdot t/\pi)},$$

$$s_3(t) = 1 + \frac{25}{128}(s_1(t) + s_2(t)), \quad t \in [0, 2\pi].$$

To illustrate this dynamic behavior, the final state of the three cross sections is shown in Fig. 6 (last row). The respective dynamic cone-beam data are simulated for 360 source positions rotating on a circle with radius $R = 8$ and 801×801 planar detector points. In order to account for the statistical nature of photon emission, we further add noise to the simulated data characterized by the Poisson distribution resulting in an overall peak-signal-to-noise-ratio of 16 dB (corresponding to a noise level of approximately 6%).

We then apply the proposed dynamic algorithm with regularization parameters $\gamma = 0.0025$ and $\alpha = 1$. We further choose $L_1 = \frac{R-1}{2}$ and $L_2 = 2R$.

(continued)
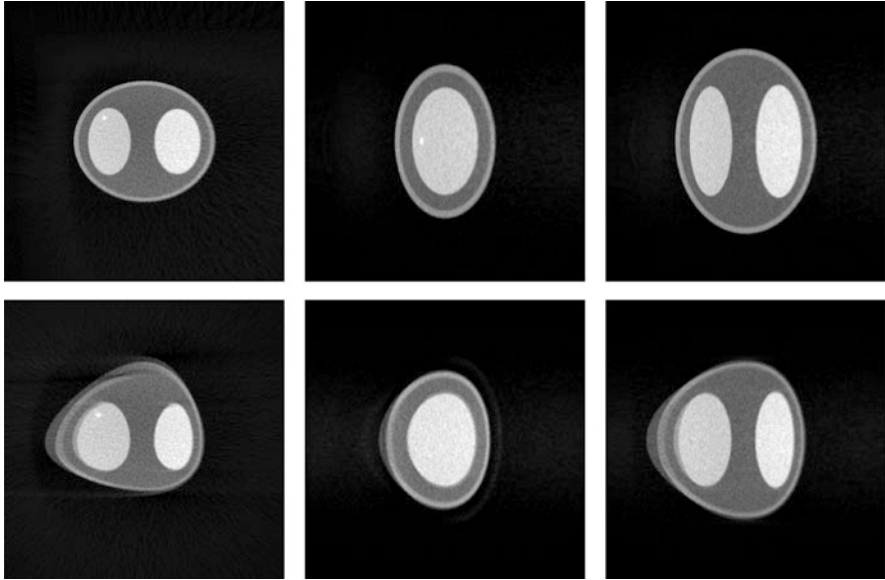
Fig. 7 Dynamic reconstruction (first row) and static reconstruction (second row) from noisy dynamic data. The three columns correspond to different crossections of the phantom (first column: fixed component $x_3 = 0$, second column: fixed component $x_2 = -0.27$, third column: fixed component $x_1 = 0$)

The respective reconstruction result is shown in Fig. 7 (first row) for the three cross sections of the object. As a comparison, the second row of Fig. 7 depicts the respective result when the algorithm with the static filter from [33] with regularization parameter $\gamma = 0.0025$ is applied to the dynamic data. Comparing the results highlights the motion compensation property of the proposed dynamic reconstruction approach. Despite the severe non-affine displacement during the data collection, the initial state is reconstructed without distortions or motion artefacts. With a static algorithm however, severe distortions arise. In particular, the small inclusion in the right ellipse (see first and second column) is not visible in the static reconstruction for $x_2 = -0.27$ (since it moved out from this cross section in the course of the data acquisition). In practical applications, the motion parameters have to be extracted beforehand, see our discussion in Sect. 2.1. Thus, we further want to evaluate how

(continued)

our dynamic reconstruction strategy performs in combination with a potential motion estimation procedure. For this purpose, we apply the dynamic reconstruction algorithm with approximate motion parameters, which are obtained by adding noise samples uniformly distributed in $[-0.09, 0.09]$ to the exact parameters. These noise samples correspond to a relative estimation error of 12, 5%. Figure 8 provides a visual comparison between the exact motion parameter s_1 and the noisy version used for the reconstruction step.

The result of the dynamic algorithm with approximate motion parameters is displayed in Fig. 9. This experiment shows that the dynamic regularization technique compensates well for the motion even if its parameters are not exactly known.
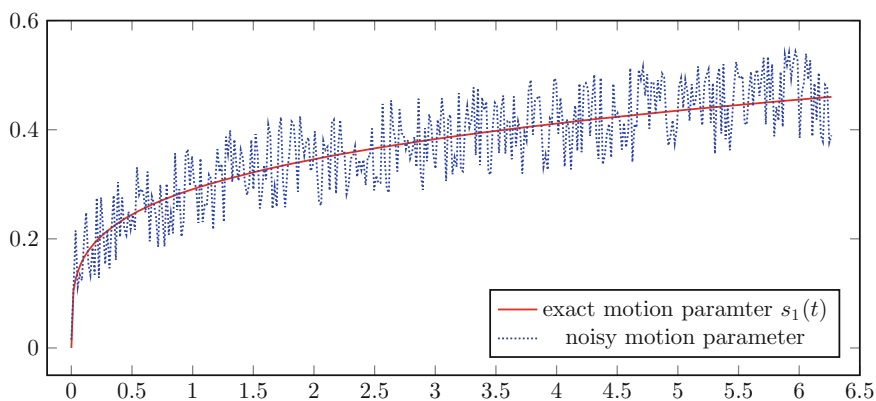
Fig. 8 Motion parameter $s_1(t)$ for $t \in [0, 2\pi]$ (solid line) and its noisy version (dashed line)
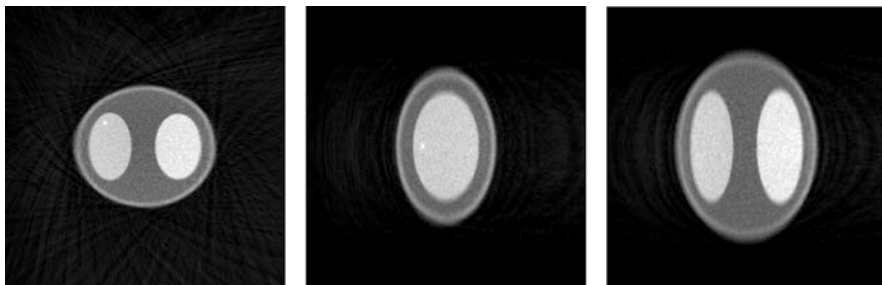
Fig. 9 Dynamic reconstruction with noisy motion parameters with nonaffine deformation from noisy dynamic data. The three columns correspond to different crossections of the phantom (first column: fixed component $x_3 = 0$, second column: fixed component $x_2 = -0.27$, third column: fixed component $x_1 = 0$)

5 Conclusion

In this chapter, we presented regularization strategies to solve general linear dynamic inverse problems with known object motion. In particular, our method based on the approximate inverse is not restricted to affine deformations. The numerical results from 3D cone-beam tomography illustrate its capability to compensate for strong, non-affine motion. The subsequent chapter provides a complementary study on the effect of the motion on the overall information content in dynamic data.

References

1. C. Blondel, R. Vaillant, G. Malandain, N. Ayache, 3D tomographic reconstruction of coronary arteries using a precomputed 4D motion field. Phys. Med. Biol. **49**, 2197–2208 (2004)
2. R. Boutchko, V.L. Rayz, N.T. Vandehey, J.P. O'Neil, T.F. Budinger, P.S. Nico, W.W. Moses, Imaging and modeling of flow in porous media using clinical nuclear emission tomography systems and computational fluid dynamics. J. Appl. Geochem. **76**, 74–81 (2012)
3. M. Burger, J. Modersitzki, S. Suhr, A nonlinear variational approach to motion-corrected reconstruction of density images. arXiv (2015)
4. C. Chen, B. Gris, O. Öktem, A new variational model for joint image reconstruction and motion estimation in spatiotemporal imaging. SIAM J. Imaging Sci. **12**, 1686–1719 (2019)
5. D. Chen, H. Li, Q. Wang, P. Zhang, Y. Zhu, Computed tomography for high-speed rotation object. Opt. Express **23**, 13423–13442 (2015)
6. J. Chung, A.K. Saibaba, M. Brown, E. Westman, Efficient generalized Golub–Kahan based methods for dynamic inverse problems. Inverse Prob. **34**, 024005 (2018)
7. C.R. Crawford, K.F. King, C.J. Ritchie, J.D. Godwin, Respiratory compensation in projection imaging using a magnification and displacement model. IEEE Trans. Med. Imaging **15**, 327–332 (1996)
8. L. Desbat, S. Roux, P. Grangeat, Compensation of some time dependent deformations in tomography. IEEE Trans. Med. Imaging **26**, 261–269 (2007)
9. R.L. Ehman, M.T. McNamara, M. Pallack, H. Hricak, C.B. Higgins, Magnetic resonance imaging with respiratory gating: techniques and advantages. Am. J. Roentgenol. **143**, 1175–1182 (1984)
10. L. Feng, M.B. Srichai, R.P. Lim, A. Harrison, W. King, G. Adluru, E.V. Dibella, D.K. Sodickson, R. Otazo, D. Kim, Highly accelerated real-time cardiac cine MRI using k-t SPARSE-SENSE. Magn. Reson. Med. **70**, 64–74 (2013)
11. D. Finch, M. Haltmeier, Rakesh, Inversion of spherical means and the wave equation in even dimensions. SIAM J. Appl. Math. **68**, 392–412 (2007)
12. J. Fitzgerald, P.G. Danias, Effect of motion on cardiac SPECT imaging: recognition and motion correction. J. Nucl. Cardiol. **8**, 701–706 (2001)
13. E. Gravier, Y. Yang, M. Jin, Tomographic reconstruction of dynamic cardiac image sequences. IEEE Trans. Image Process. **16**, 932–942 (2007)
14. B. Hahn, Reconstruction of dynamic objects with affine deformations in dynamic computerized tomography. J. Inverse Ill-Posed Prob. **22**, 323–339 (2014)

15. B.N. Hahn, Efficient algorithms for linear dynamic inverse problems with known motion. Inverse Prob. **30**, 035008 (2014)
16. B.N. Hahn, Dynamic linear inverse problems with moderate movements of the object: ill-posedness and regularization. Inverse Prob. Imaging **9**, 395–413 (2015)
17. B.N. Hahn, Motion estimation and compensation strategies in dynamic computerized tomography. Sensing Imaging **18** 1–20 (2017)
18. B. N. Hahn, E.T. Quinto, Detectable singularities from dynamic Radon data. SIAM J. Imaging Sci. **9**, 1195–1225 (2016)
19. B.N. Hahn, M.L. Kienle-Garrido, E.T. Quinto, Microlocal properties of dynamic Fourier integral operators, in *Time-Dependent Problems in Imaging and Parameter Identification*, ed. by B. Kaltenbacher, T. Schuster, A. Wald (Springer, Cham, 2021), pp. 85–120
20. B.N. Hahn, A.K. Louis, M. Maisl, C. Schorr, Combined reconstruction and edge detection in dimensioning. Meas. Sci. Technol. **24**, 125601 (2013)
21. A.A. Isola, A. Ziegler, T. Koehler, W.J. Niessen, M. Grass, Motion-compensated iterative cone-beam CT image reconstruction with adapted blobs as basis functions. Phys. Med. Biol. **53**, 6777–6797 (2008)
22. J. Kastner, B. Plank, C. Heinzl, Advanced X-ray computed tomography methods: high resolution CT, phase contrast CT, quantitative CT and 4DCT, in *Proceedings: Digital Industrial Radiology and Computed Tomography (DIR 2015), Ghent* (2015)
23. A. Katsevich, An accurate approximate algorithm for motion compensation in two-dimensional tomography. Inverse Prob. **26**, 065007 (2010)
24. A. Katsevich, M. Silver, A. Zamayatin, Local tomography and the motion estimation problem. SIAM J. Imaging Sci. **4**, 200–219 (2011)
25. S. Kindermann, A. Leitão, On regularization methods for inverse problems of dynamic type. Numer. Funct. Anal. Optim. **27**, 139–160 (2006)
26. P. Kuchment, L. Kunyansky, Mathematics of photoacoustic and thermoacoustic tomography, in *Handbook of Mathematical Methods in Imaging*, ed. by O. Scherzer (Springer, New York, 2015)
27. D. Le Bihan, C. Poupon, A. Amadon, F. Lethimonnier, Artifacts and pitfalls in diffusion MRI. J. Magn. Reson. Imaging **24**, 478–488 (2006)
28. S. Lingala, E. DiBella, M. Jacob, Deformation corrected compressed sensing (DC-CS): a novel framework for accelerated dynamic MRI. IEEE Trans. Med. Imaging **34**, 72–85 (2015)
29. J. Liu, X. Zhang, X. Zhang, H. Zhao, Y. Gao, D. Thomas, D.A. Low, H. Gao, 5D respiratory motion model based image reconstruction algorithm for 4D cone-beam computed tomography. Inverse Prob. **31**, 115007 (2015)
30. A.K. Louis, Approximate inverse for linear and some nonlinear problems. Inverse Prob. **12**, 175–190 (1996)
31. A.K. Louis, Feature reconstruction in inverse problems. Inverse Prob. **27**, 065010 (2011)
32. A.K. Louis, P. Maass, A mollifier method for linear operator equations of the first kind. Inverse Prob. **6**, 427–440 (1990)
33. A.K. Louis, T. Weber, D. Theis, Computing reconstruction kernels for circular 3D cone beam tomography. IEEE Trans. Med. Imaging **27**, 880–886 (2008). Special Issue on Fully 3D Image Reconstruction
34. W. Lu, T.R. Mackie, Tomographic motion detection and correction directly in sinogram space. Phys. Med. Biol. **47**, 1267–84 (2002)
35. D. Manke, K. Nehrke, P. Börnert, Novel prospective respiratory motion correction approach for free-breathing coronary MR angiography using a patient-adapted affine motion model. Magn. Reson. Med. **50**, 122–131 (2003)
36. S.J. McQuaid, B.F. Hutton, Sources of attenuation-correction artefacts in cardiac PET/CT and SPECT/CT. Eur. J. Nucl. Med. Mol. Imaging **35**, 1117–1123 (2008)
37. F. Natterer, F. Wübbeling, *Mathematical Methods in Image Reconstruction* (SIAM, Philadelphia, 2011)
38. E. Niemi, M. Lassas, A. Kallonen, L. Harhanen, K. Hämäläinen, S. Siltanen, Dynamic multi-source X-ray tomography using a spacetime level set method. J. Comput. Phys. **291**, 218–237 (2015)

39. R. Otazo, E. Candès, D.K. Sodickson, Low-rank plus sparse matrix decomposition for accelerated dynamic MRI with separation of background and dynamic components. Magn. Reson. Med. **73**, 1125–1136 (2015)
40. M. Reyes, G. Malandain, P.M. Koulibaly, M.A. González-Ballester, J. Darcourt, Model-based respiratory motion compensation for emission tomography image reconstruction. Phys. Med. Biol. **52**, 3579–3600 (2007)
41. S. Rit, D. Sarrut, L. Desbat, Comparison of analytic and algebraic methods for motion-compensated cone-beam CT reconstruction of the thorax. IEEE Trans. Med. Imaging **28**, 1513–1525 (2009)
42. E.L. Ritman, J.H. Kinsey, R.A. Robb, L.D. Harris, B.K. Gilbert, Physical and technical considerations in the design of the DSR: A high temporal resolution volume scanner. Am. J. Roentgenol. **134**, 369–374 (1980)
43. S. Roux, L. Desbat, A. Koenig, P. Grangeat, Exact reconstruction in 2D dynamic CT: compensation of time-dependent affine deformations. Phys. Med. Biol. **49**, 2169–2182 (2004)
44. U. Schmitt, A.K. Louis, Efficient algorithms for the regularization of dynamic inverse problems: I. Theory. Inverse Prob. **18**, 645–658 (2002)
45. U. Schmitt, A.K. Louis, C. Wolters, M. Vauhkonen, Efficient algorithms for the regularization of dynamic inverse problems: II. Applications. Inverse Prob. **18**, 659–676 (2002)
46. T. Schuster, *The Method of Approximate Inverse: Theory and Applications* (Springer, Berlin, 2007)
47. L. Shepp, S. Hilal, R. Schulz, The tuning fork artifact in computerized tomography. Comput. Graphics Image Process. **10**, 246–255 (1979)
48. R.M. Temam, A.M. Miranville, *Mathematical Modeling in Continuum Mechanics* 2nd edn. (Cambridge University Press, New York, 2005)
49. T. Weber, Schnelle Rekonstruktionskernberechnung in der 3D-Computertomographie. Ph.D. thesis, Saarland University (2008)
50. R. Zeng, J.A. Fessler, J.M. Balter, Respiratory motion estimation from slowly rotating x-ray projections: theory and simulation. Med. Phys. **32**, 984–991 (2005)